https://doi.org/10.5194/amt-2019-432
Preprint. Discussion started: 2 January 2020

Atmospheric Measurement Techniques Discussions

First validation of Aeolus wind observations by airborne Doppler Wind Lidar measurements

Benjamin Witschas[1], Christian Lemmerz[1], Alexander Geiß[2], Oliver Lux[1], Uwe Marksteiner[1], Stephan Rahm[1], Oliver Reitebuch[1], and Fabian Weiler[1]

[1]Deutsches Zentrum für Luft- und Raumfahrt e.V. (DLR), Institut für Physik der Atmosphäre, 82234 Oberpfaffenhofen, Germany
[2]Ludwig-Maximilians-Universität, Meteorologisches Institut, 80333 München, Germany

Correspondence: Benjamin Witschas, (Benjamin.Witschas@dlr.de)

Abstract. Soon after the launch of Aeolus on 22 August 2018, the first ever wind lidar in space developed by the European Space Agency (ESA) has been providing profiles of the component of the wind vector along the instrument's line-of-sight (LOS) on a global scale. In order to validate the quality of Aeolus wind observations, the German Aerospace Center (Deutsches Zentrum für Luft- und Raumfahrt e.V., DLR) recently performed two airborne campaigns over Central Europe deploying two different Doppler wind lidars (DWL) on-board the DLR Falcon aircraft. The first campaign - WindVal III - was conducted from 5 November 2018 until 5 December 2018 and thus, still within the commissioning phase of the Aeolus mission. The second campaign - AVATARE (Aeolus Validation Through Airborne Lidars in Europe) - was performed from 6 May 2019 until 6 June 2019. Both campaigns were flown out of the DLR site in Oberpfaffenhofen, Germany. All together, 10 satellite underflights with 19 flight legs covering more than 7500 km of Aeolus swaths were performed and used to validate the early stage wind data product of Aeolus by means of collocated airborne wind lidar observations for the first time. For both campaign data sets, the statistical comparison of Aeolus data and the data of the reference lidar (2-μm DWL) on-board the Falcon aircraft shows enhanced systematic and random errors compared with the bias and precision requirements defined for Aeolus. In particular, the systematic errors are determined to be 2.1 m/s (Rayleigh) and 2.3 m/s (Mie) for WindVal III and -4.6 m/s (Rayleigh) and -0.2 m/s (Mie) for AVATARE. The corresponding random errors are determined to be 4.0 m/s (Rayleigh) and 2.2 m/s (Mie) for WindVal III, and 4.4 m/s (Rayleigh) and 2.2 m/s (Mie) for AVATARE. Potential reasons for those errors are analyzed and discussed.

1 Introduction

Since 22 August 2018, the first European spaceborne lidar and the first ever spaceborne Doppler wind lidar, Aeolus, developed by ESA has been circling on its sun-synchronous orbit at about 320 km altitude (ESA, 1999). Aeolus is carrying a single payload, namely the Atmospheric Laser Doppler Instrument (ALADIN) which provides profiles of the component of the wind vector along the instruments LOS direction on a global scale from ground up to about 30 km in the stratosphere (ESA, 1999; Stoffelen et al., 2005; Reitebuch, 2012; Kanitz et al., 2019). With that, the Aeolus mission is primarily aiming to improve

https://doi.org/10.5194/amt-2019-432
Preprint. Discussion started: 2 January 2020

Atmospheric Measurement Techniques Discussions

Numerical Weather Prediction (NWP) and medium-range weather forecast (e.g., Weissmann and Cardinali, 2007; Tan et al., 2007; Marseille et al., 2008; Horányi et al., 2015).

ALADIN is a direct detection wind lidar operating at a laser wavelength of 354.8 nm and is able to retrieve LOS wind speeds by exploiting the Doppler shift of light backscattered from molecules and from particles. In order to do so, ALADIN is equipped with two different frequency discriminators, namely a Fizeau interferometer that is used to analyze the frequency shift of the narrow-band particulate return signal by means of the so-called fringe imaging technique (McKay, 2002), and two coupled Fabry-Perot interferometers that are used to analyze the frequency shift of the broad-band molecular return signal by the so-called double edge technique (e.g., Chanin et al., 1989; Flesia and Korb, 1999). This high-spectral resolution receiver configuration also provides the possibility to retrieve information on the vertical distribution of aerosol and cloud optical properties such as backscatter and extinction coefficients (Ansmann et al., 2007; Flamant et al., 2008).

The direct detection measurement principle requires regular instrument calibration, a stable instrument alignment and further post-processing that relates the measured signal levels to a frequency Doppler shift which can then be translated into a wind speed (Dabas et al., 2008; Lux et al., 2018; Marksteiner et al., 2018; Zhai et al., 2019). Hence, especially the accuracy of wind speeds retrieved from direct detection wind lidars is strongly depending on the aforementioned points. This also means that a validation of Aeolus winds by means of independent ground-based and airborne measurements is inevitable. For that reason, ESA already provided preliminary Aeolus data in a very early stage of the mission (since 16 December 2018) to approved Cal/Val teams that especially perform ground-based and airborne measurements for validation purpose (https://aeolus-ds.eo.esa.int/oads/access/).

As one of these teams, DLR recently performed two airborne campaigns over Central Europe namely the WindVal III campaign and the AVATARE campaign with the DLR Falcon research aircraft equipped with two wind lidar systems that have been deployed in several Aeolus pre-launch campaigns within the last 10 years (Marksteiner, 2013; Marksteiner et al., 2018; Schäfler et al., 2018; Lux et al., 2018). During both campaigns, 10 satellite underflights covering more than 7500 km of Aeolus swaths were acquired. Based on these measurements, this paper presents the first validation of the early stage Aeolus horizontal-line-of-sight (HLOS) wind product (Level 2B). In particular, the Aeolus data is compared to 2-μm DWL measurements which act as a reference due to their low systematic and random errors that come along with the coherent measurement principle of the system. A study of the Aeolus measurement principle, its calibration procedures and retrieval algorithms is performed based on ALADIN airborne demonstrator (A2D) observations as discussed in Lux et al. (2019).

First an overview of the two validation campaigns is given, followed by a discussion of the ALADIN and 2-μm DWL instrumental setup and measurement schemes. Afterwards, the procedure of matching the different resolutions of the used data sets is explained and a statistical comparison is performed. Finally, potential reasons for the observed enhanced systematic and random errors of Aeolus winds are discussed.

https://doi.org/10.5194/amt-2019-432
Preprint. Discussion started: 2 January 2020

Atmospheric Measurement Techniques Discussions

2 Validation campaigns overview

Still within the commissioning phase of Aeolus, DLR performed a first airborne Aeolus validation campaign (WindVal III) from the site in Oberpfaffenhofen, Germany in the timeframe from 5 November 2018 to 5 December 2018. Half a year later, a second airborne Aeolus validation campaign called AVATARE was conducted from 6 May 2019 until 6 June 2019. During both

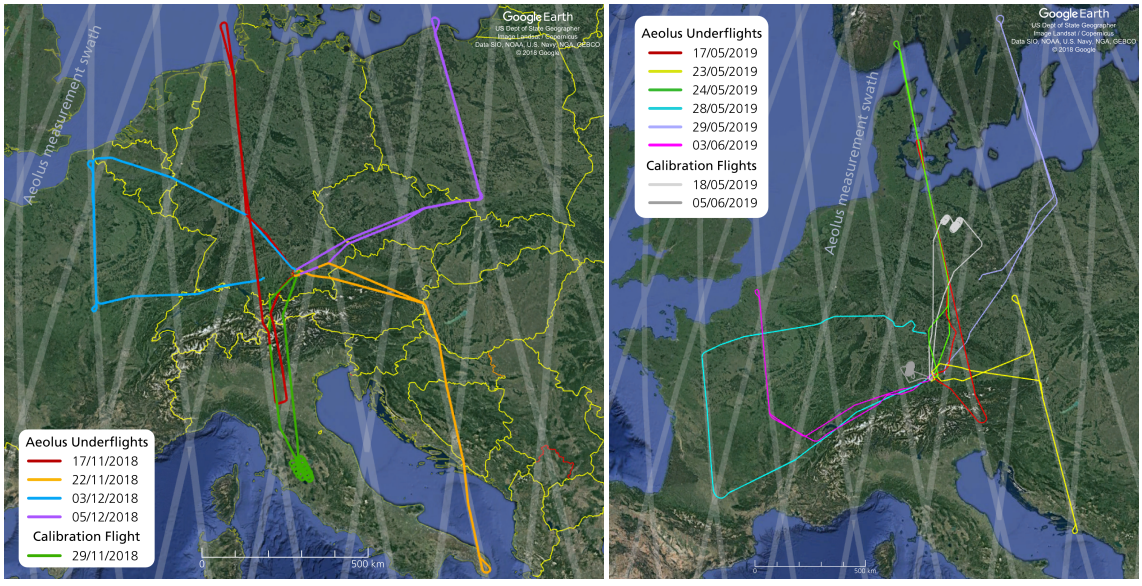

Figure 1. Flight tracks of the Falcon aircraft during the WindVal III campaign performed from 17 November 2018 to 5 December 2018 (left) and the AVATARE campaign performed from 17 May 2019 to 3 June 2019 (right). Each color represents a single flight. The Aeolus measurement swath is shown in gray color. During the probed evening satellite tracks, the Aeolus moving direction was always from south to north (ascending orbit).

campaigns, the DLR Falcon was equipped with two wind lidar systems that have been deployed in several Aeolus pre-launch campaigns as for instance the WindVal I campaign (Marksteiner et al., 2018) and the WindVal II campaign (Schäfler et al., 2018; Lux et al., 2018) both flown out of Keflavik, Iceland. In particular, the Falcon hosted the A2D which is a prototype of the ALADIN instrument with representative design and measurement principle (Reitebuch et al., 2009). The A2D was developed by the former European Defence and Space Company (EADS-Astrium - now Airbus Defence and Space) together with DLR in order to validate the ALADIN measurement principle, calibration procedures, retrieval algorithms and wind product quality before and after the launch of Aeolus. Additionally, a coherent detection wind lidar (2-μm DWL) with a high sensitivity to particulate returns was flown and acted as a reference system (Witschas et al., 2017)

Whereas the flights performed during WindVal I and WindVal II resulted in refinements of the Aeolus wind retrieval algorithms based on measurements performed in real atmosphere, wind observations collocated with Aeolus could be acquired during WindVal III and AVATARE, enabling the first ever validation of the early stage Aeolus HLOS winds (Level 2B). In order to do so, 4 satellite underflights composed of 8 flight legs were conducted during WindVal III over Central Europe, covering

https://doi.org/10.5194/amt-2019-432
Preprint. Discussion started: 2 January 2020

Atmospheric Measurement Techniques Discussions

more than 3000 km of Aeolus swaths. During AVATARE, 6 satellite underflights composed of 11 flight legs were performed over Central Europe covering more than 4500 km Aeolus swaths. Thus, data of 19 flight legs from 10 satellite underflights that cover more than 7500 km of Aeolus swaths are available and used for the validation Aeolus HLOS winds. An overview of the flight tracks flown during WindVal III and AVATARE is shown in Fig. 1, left and right, respectively. Further details about the flight times of the Falcon aircraft and the overflight times of Aeolus are given in Table 1.

Table 1. Overview of Aeolus underflights performed during the WindVal III and the AVATARE campaign

	Falcon flight			Aeolus underflight	
	Date	Time/(UTC)	Route	Start/stop time/(UTC)	Geolocation
WindVal III	17 Nov. 2018	15:14 to 19:14	OBF to OBF	17:01:21 to 17:03:56	44.7 °N, 10.6 °E to 54.9 °N, 7.8 °E
	22 Nov. 2018	14:29 to 17:56	OBF to OBF	16:34:14 to 16:36:02	40.0 °N, 18.3 °E to 47.2 °N, 16.5 °E
	3 Dec. 2018	15:48 to 19:31	FMM to OBF	17:27:55 to 17:28:51	47.1 °N, 3.6 °E to 50.8 °N, 2.6 °E
	3 Dec. 2018	14:56 to 18:22	OBF to OBF	16:23:50 to 16:25:02	50.2 °N, 19.0 °E to 54.9 °N, 17.5 °E
AVATARE	17 May 2019	15:36 to 18:46	OBF to OBF	16:48:39 to 16:51:01	46.3 °N, 13.4 °E to 55.5 °N, 10.7 °E
	23 May 2019	14:30 to 18:08	OBF to OBF	16:34:55 to 16:36:55	42.9 °N, 17.5 °E to 50.5 °N, 15.6 °E
	24 May 2019	15:28 to 19:09	OBF to OBF	16:50:01 to 16:52:18	51.2 °N, 12.2 °E to 59.0 °N, 9.4 °E
	28 May 2019	15:54 to 19:13	NUE to OBF	17:40:05 to 17:41:10	44.0 °N, 1.1 °E to 48.2 °N, 0.1 °E
	29 May 2019	15:26 to 19:11	OBF to OBF	16:24:40 to 16:26:12	53.5 °N, 18.1 °E to 59.4 °N, 15.9 °E
	3 Jun. 2019	15:26 to 18:46	OBF to OBF	17:27:50 to 17:28:48	46.8 °N, 3.6 °E to 50.6 °N, 2.6 °E

The time gives the duration between takeoff and landing. The flight route is indicated by the IATA (International Air Transport Association) airport code. OBF: Oberpfaffenhofen airport; FMM: Memmingen Allgäu airport; NUE: Nuremberg airport.

3 The Atmospheric Laser Doppler Instrument ALADIN on-board Aeolus

In this section, the Aeolus satellite and its instrument ALADIN are shortly introduced, including its measurements procedure and resulting data products. For more information regarding these topics please refer to (e.g., ESA, 1999; Reitebuch, 2012; Reitebuch et al., 2019; Kanitz et al., 2019; Straume et al., 2018, 2019).

3.1 Instrument description

The Aeolus satellite was launched on 22 August 2018. It has a weight of 1360 kg, a launch configuration dimension of 4.6 m x 1.9 m x 2.0 m and it can provide a power of 2.4 kW. It is flying on a 320 km sun-synchronous orbit with an inclination of 97°, leading to a 7-day repeat cycle. Aeolus carries a single payload, ALADIN, which is a direct detection wind lidar operating an ultraviolet wavelength of 354.8 nm. ALADIN emits short laser pulses (≈ 40 mJ to 70 mJ, 50.5 Hz) down to the atmosphere where a few of the photons are backscattered on air molecules, aerosols and hydrometeors. The backscattered light is collected with a 1.5 m diameter telescope and directed to the optical receiver that is used to detect the Doppler frequency shift of the

https://doi.org/10.5194/amt-2019-432
Preprint. Discussion started: 2 January 2020


Atmospheric Measurement Techniques Discussions

backscattered light and with that, the wind velocity in LOS direction at different altitudes. In order to do so, ALADIN is equipped with two different frequency discriminators, namely a Fizeau interferometer that is used to analyze the frequency shift of the narrow-band particulate backscatter signal, and two sequentially coupled Fabry-Perot interferometers that are used to analyze the frequency shift of the broad-band molecular return signal. Both, the Rayleigh and Mie channel sample the backscatter signal time resolved to 24 bins with a vertical resolution between 0.25 km and 2.0 km. The horizontal resolution of the wind observations is about 90 km for the Rayleigh channel down to 10 km for the Mie channel with an overall sub-sample information on a 3 km scale. Furthermore, due to the high-spectral resolution receiver configuration, also information on the vertical distribution of aerosol and cloud optical properties such as backscatter and extinction coefficients can be retrieved from Aeolus data (Ansmann et al., 2007; Flamant et al., 2008).

As demonstrated by several authors (e.g., Reitebuch et al., 2014; Lux et al., 2018; Marksteiner et al., 2018; Zhai et al., 2019), the direct detection measurement principle requires regular instrument calibration and further post-processing that relates the measured signal levels to a frequency Doppler shift which can then be converted into a wind speed. Hence, especially the systematic error of wind speeds retrieved from direct detection wind lidars is strongly depending on the quality of the instrument calibration and the alignment stability of the instrument itself. Thus, in order to verify if the Aeolus instrument calibration procedures and processing steps are robust, validation measurements are inevitable.

3.2 Aeolus data products

The Aeolus data processing chain offers different data product levels containing different types of information. A short overview of them is given in this section. For additional information it is referred to (e.g., Tan et al., 2008; ESA, 2016; Tan et al., 2017; Rennie, 2018).

The Level 0 data contains the raw data of ALADIN as well as the instrument housekeeping data and the housekeeping data of the satellite platform. The assignment of the geolocation to each measurement and the full processing of the satellite housekeeping data is done in the Level 1A processor. The Level 1B data already provides processed ground echo data and preliminary HLOS wind observation that have not been corrected for atmospheric temperature and pressure (Reitebuch et al., 2018). Additionally, the viewing geometry data is available (Tan et al., 2008). The Level 2B data contains the time series of fully processed profiles of HLOS wind along the satellite orbit. It is the data product that is also used by the European Centre for Medium-Range Weather Forecasts (ECMWF) for NWP (Tan et al., 2017; Rennie, 2018) and for the validation by means of 2-μm DWL measurements as discussed later. It is worth mentioning that the sign of the HLOS winds is defined such that it is positive for winds blowing away from the satellite. For instance, for an ascending orbit, when the satellite moves from south to north and the laser is pointing east-wards, westerly winds lead to positive HLOS winds.

Additionally, there is also Level 2C data available which contains the time series of three-dimensional wind vector profiles along the satellite track, which are produced by the ECMWF model after ingestion of Level 2B data.

From Level 1B to Level 2B, the following important steps are performed. First, the single measurements are grouped into observations. By doing so, the horizontal resolution and the noise of the respective wind observation are controlled. Furthermore, the measurements are classified by means of the optical properties of the atmosphere. In particular, the wind observations

https://doi.org/10.5194/amt-2019-432
Preprint. Discussion started: 2 January 2020


Atmospheric Measurement Techniques Discussions

are classified into Rayleigh-clear winds, indicating wind observations in aerosol-poor atmosphere and Mie-cloudy winds, indicating winds acquired from particulate backscatter, predominately from clouds. There are also Rayleigh-cloudy and Mie-clear winds available in the data product which are not further discussed within this study. Moreover, a temperature and pressure correction is applied for the Rayleigh-wind retrieval which is needed in order to avoid systematic errors (Dabas et al., 2008). As the Rayleigh-Brillouin spectrum of molecular scattered light depends on temperature and pressure (Witschas et al., 2010; Witschas, 2011a, b; Witschas et al., 2014), any temperature and pressure differences between instrument response calibration and wind observation have to be taken into account. Additionally, a potential cross-talk between the Mie and the Rayleigh channel is corrected within the Level 2B processor. Rayleigh-clear winds are usually retrieved for a backscatter ratio from 1.0 to 1.4, where the backscatter ratio is defined as the ratio of the total backscatter coefficient (particles and molecules) to the molecular component. Thus, for the larger scattering ratios (close to 1.4) the sensitivity of the Rayleigh channel might already be impacted by the enhanced Mie signal which has to be considered for the wind retrieval in order to avoid systematic errors. Besides these processing steps, uncertainty estimates and quality flags are calculated for each wind observation and can be used for quality control.

It is worth mentioning that the Level 2B HLOS winds used in this study are still on a early stage state. The Level 1B and Level 2B processors are continuously updated and particular improvements have already been performed; however, the satellite data has not been re-processed yet. For the Level 2B HLOS winds analyzed here, one and the same instrument calibration file was used from start of the mission until 16 May 2019. Additionally, ECMWF model comparisons from September 2018 were used to further correct a remaining systematic bias. On 16 May 2019, the calibration file was updated. Thus, the two campaigns discussed here, are comparing to Aeolus data processed with different instrument calibration files. Another difference between both campaigns is the resolution of Mie winds. On 5 March 2019 (8:44 UTC), the resolution of Mie winds was increased by decreasing the horizontal averaging down to about 10 km. Furthermore, the range-gate settings of Aeolus were changed on 26 February 2019 (00:00 UTC) such that they follow the ground elevation which also increases the number of available data points.

4 The 2-μm Doppler Wind Lidar at DLR

The 2-μm DWL has been operating by DLR for almost 20 years and has been deployed in several ground and airborne field campaigns for measuring aircraft wake vortices (Köpp et al., 2004), aerosol optical properties (Chouza et al., 2015, 2017), horizontal wind speeds over the Atlantic Ocean as input data for assimilation experiments (Weissmann et al., 2005; Schäfler et al., 2018) and horizontal and vertical wind speeds to study the life cycle of gravity waves (Witschas et al., 2017). In addition to that, the system was applied in several Aeolus pre-launch campaigns conducted within the last 10 years (e.g., Marksteiner et al., 2018; Lux et al., 2018).

In this section, the 2-μm DWL instrument is shortly described, followed by an explanation of the corresponding measurement procedure and wind retrieval algorithm. Afterwards, the accuracy and precision of the derived wind speeds are discussed by means of comparison to dropsonde measurements available from previous campaigns.

https://doi.org/10.5194/amt-2019-432
Preprint. Discussion started: 2 January 2020


Atmospheric Measurement Techniques Discussions

4.1 Instrument description

The 2-μm DWL is a coherent detection wind lidar system based on a Tm:LuAG laser operating at a wavelength of 2022.54 nm (vacuum), a laser pulse energy of 1 mJ to 2 mJ and a pulse repetition rate of 500 Hz, insuring eye-safe operation. The system was built by CLR Photonics (today Lockheed Martin Coherent Technologies) and has been deployed at DLR since October 1999.

The 2-μm DWL is composed of three units, namely (1) a transceiver head containing the laser, a 11 cm afocal telescope, receiver optics, detectors and a double wedge scanner enabling to steer the laser beam to any position within a 30° cone angle; (2) a power supply and the cooling unit of the laser, mounted in a separate rack; and (3) a rack containing the data acquisition unit and the control electronics, developed by DLR. For a more detailed description of the 2-μm DWL including a listing of the system specifications it is referred to Witschas et al. (2017).

4.2 Measurement procedure and wind retrieval

In order to measure the three-dimensional wind speed and direction, the velocity-azimuth display (VAD) scan technique is applied (Browning and Wexler, 1968). That is, a conical step-and-stare scan around the vertical axes with an off-nadir angle of 20° is performed for 21 LOS positions, separated by 18° in azimuth direction. Considering a 1 s averaging time for each LOS measurement and an additional second in order to change the laser beam pointing direction, one scanner revolution takes about 42 s. By further taking into account the aircraft speed of about 200 m/s, the horizontal resolution of 2-μm DWL wind observations is about 8.4 km, depending on the actual ground speed of the aircraft. The vertical resolution of the wind observations is determined by the laser pulse length and the averaging interval which is set to be 100 m.

In order to retrieve wind speed and wind direction profiles from the single LOS measurements performed during one scanner revolution, several techniques are available (Smalikho, 2003). As discussed by Witschas et al. (2017), an algorithm based on a maximum function of accumulated spectra (MFAS) is used as baseline for the 2-μm DWL. The MFAS algorithm retrieves wind speed and wind direction without estimating single LOS wind velocities and thus yields valid wind estimates even in regions of low signal-to-noise ratios (SNR). In particular, the spectra of all 21 LOS measurements are shifted to be proportional to their azimuth angle and an assumed wind vector. Afterwards, all spectra are accumulated and the maximum of the accumulated spectra is determined. For a correctly assumed wind vector, the accumulated spectra have a maximum and thus indicate the prevailing wind vector. By applying the MFAS algorithm to one scanner revolution, the horizontal and vertical resolution of the retrieved wind vectors is about 8.4 km and 100 m, respectively.

Considering the lower resolution of Aeolus data, which is about 90 km for the Rayleigh-clear winds and down to 10 km for the Mie-cloudy winds (horizontal) and between 0.5 km and 2 km (vertical), it was investigated if an increased number of averaged spectra for the MFAS-algorithm could further improve the 2-μm DWL data coverage and with that, increase the number of data points available for comparison to Aeolus observations. In particular, a floating window of 5 scanner revolutions (90 LOS measurements) and 5 range gates (500 m) is used, decreasing the effective horizontal and vertical resolution of the retrieved wind vectors to 42 km and 500 m, respectively.

https://doi.org/10.5194/amt-2019-432
Preprint. Discussion started: 2 January 2020

Atmospheric Measurement Techniques Discussions

In Fig. 2, an example of the wind speed retrieved from 2-μm DWL measurements performed on the first flight leg of the first ever Aeolus underflight performed on 17 November 2018 during the WindVal III campaign is shown. The flight leg ranges from 44.85°N to 54.82°N which corresponds to a track length of 1146 km. The leg started south of the Alps at 15:57 UTC and ended in the north of Germany at 17:45 UTC (see also Fig. 1, left, red line). The Aeolus overflight was at around 17:02 UTC. The top panel indicates data processed with the MFAS algorithm for one scanner revolution and 100 m vertical resolution, the bottom panel shows data processed with the MFAS algorithm for five scanner revolutions and 500 m vertical resolution, respectively. It can be seen that the data coverage for the five-scanner-revolution average is remarkably increased. In particular,

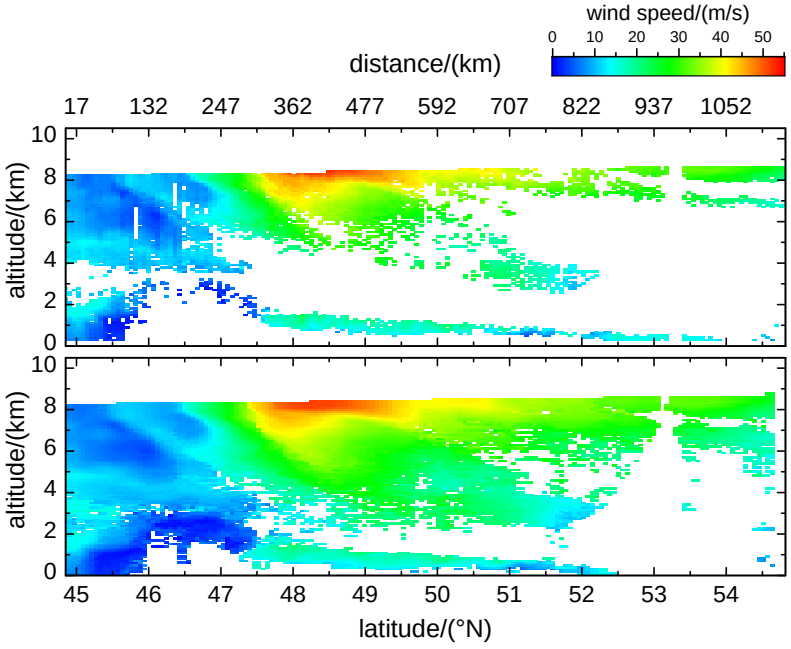

Figure 2. Wind speed retrieved from 2-μm DWL data by means of the MFAS algorithm for one scanner revolution (top) and five scanner revolutions (bottom), respectively during the first ever Aeolus underflight performed on 17 November 2018 during the WindVal III campaign (see also Table 1 and Fig. 1, left, red line). The flight leg ranges from 44.85°N to 54.82°N which corresponds to 1146 km track length. The leg started in the south at 15:57 UTC and ended in the north at 17:45 UTC. The satellite overflight was at around 17:02 UTC. White colors indicate areas with no valid wind measurements due to aerosol-poor atmospheric conditions and a corresponding insufficient SNR.

the retrieval by means of one scanner revolution yields 4693 valid data points out of 12517 data points which would give full coverage. Thus, the data coverage with one scanner revolution is about 37.5%. On the other hand, the retrieval by means of five scanner revolutions yields 8719 valid data points which corresponds to a data coverage of 70% and thus an increase of 86% compared to the one scanner revolution. Apart from that it can be seen that detailed structures, for instance in the vicinity of the jet-stream (47.5°N to 50.0°N), get less pronounced or rather blurred due to the decreased resolution of the data. However, as the resolution of the satellite data is even coarser, this is not an issue for comparison. For that reason, the 2-μm DWL data

https://doi.org/10.5194/amt-2019-432
Preprint. Discussion started: 2 January 2020


Atmospheric Measurement Techniques Discussions

retrieved by means of the modified MFAS algorithm using five scanner resolutions (horizontal) and five range gates (vertical) is used for comparison to Aeolus observations as it increases the number of available data points significantly. For all flight legs performed during WindVal III and AVATARE, 56% more data is available when applying the five-scanner-revolution average, keeping all the other parameters constant.

4.3 Accuracy and precision of the retrieved wind speed

In order to asses the accuracy (systematic error) and precision (random error) of 2-μm DWL wind measurements, comparisons to dropsonde data were performed during several campaigns within the past years (Weissmann et al., 2005; Chouza et al., 2016; Reitebuch et al., 2017; Schäfler et al., 2018), and power spectra of LOS winds were analyzed (Witschas et al., 2017).

During the Gravity Wave Life-Cycle (GW-LCYCLE) I campaign (Wagner et al., 2017), the 2-μm DWL was used to measure horizontal and vertical wind speeds in order to investigate the life cycle of internal gravity waves induced by flow across the Scandinavian mountains. The spectral power of the vertical winds measured on a flight performed on 13 December 2013 in 5 km altitude indicate that the mean random error of LOS winds is 0.21 m/s and the mean systematic error of LOS winds is estimated to be smaller than 0.05 m/s (Witschas et al., 2017).

In addition, the random and systematic error of 2-μm DWL wind speed measurements were determined by means of comparisons to dropsonde data. In particular, the data set acquired during the A-TreC campaign (Weissmann et al., 2005), the SALTRACE campaign (Chouza et al., 2016), the WindVal I campaign (Reitebuch et al., 2017) and the NAWDEX campaign (Schäfler et al., 2018) was used to determine the systematic error of retrieved wind speeds to be always below 0.1 m/s and the random error to vary between 0.92 m/s and 1.5 m/s. It is worth mentioning that both the systematic and the random error are composed of the contribution of the 2-μm DWL and the dropsonde. An overview of the respective results is given in Table 2.

The variability of the systematic and the random error for different campaign data sets can have several reasons as for instance slightly different thresholds for the allowed spatial and temporal distance between dropsonde and lidar observation and slightly different quality controls for the dropsonde and lidar measurements. Nevertheless, considering the low systematic error of smaller than 0.1 m/s and a reasonable random error varying between 0.92 m/s and 1.5 m/s it can be concluded that the 2-μm DWLis a suitable reference instrument for Aeolus validation.

5 Comparison of Aeolus and 2-μm Doppler Wind Lidar data

Due to the different horizontal and vertical resolutions of 2-μm DWL measurements ($\approx$ 8.4 km, 100 m for one scanner revolution or rather $\approx$ 42 km, 500 m) and Aeolus measurements ($\approx$ 90 km (Rayleigh) and down to $\approx$ 10 km (Mie), 0.25 km to 2 km), averaging procedures are needed in order to compare respective wind observations. Furthermore, as Aeolus is only providing HLOS winds, the 2-μm DWL measurements have to be projected onto the Aeolus HLOS direction. A sketch of the applied processing steps is shown in Fig. 3. First, the wind speed and wind direction measured by the 2-μm DWL are averaged to the Aeolus grid by using the top and bottom altitudes as well as the start and stop latitudes given in the Aeolus

https://doi.org/10.5194/amt-2019-432
Preprint. Discussion started: 2 January 2020

Atmospheric Measurement Techniques Discussions

Table 2. Systematic and random error of 2-μm DWL wind speeds determined by comparison to dropsonde measurements and power spectrum analysis of LOS winds.

Wind product	Systematic error	Random error	Data points	Reference
Horizontal wind speed	0.00 m/s	1.20 m/s	740	Weissmann et al. (2005)
Horizontal wind speed	0.08 m/s	0.92 m/s	1329	Chouza et al. (2016)
Horizontal wind speed	0.03 m/s	1.46 m/s	938	Reitebuch et al. (2017)
Horizontal wind speed	0.05 m/s	1.50 m/s	245	Schäfler et al. (2018)
Single LOS wind speed	0.05 m/s	0.20 m/s	2000	Witschas et al. (2017)

Both the random error and the systematic error are composed of the contribution of the 2-μm DWL and the dropsondes.

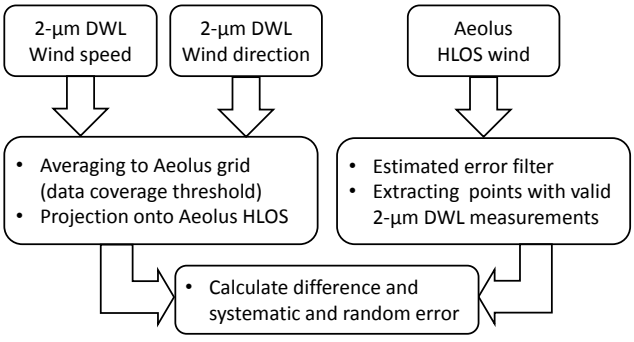

Figure 3. Sketch of the processing steps used to compare 2-μm DWL measurements with Aeolus observations.

Level 2B data product. As the 2-μm DWL does not provide full data coverage, a threshold for the number of available 2-μm DWL observations within an Aeolus grid point has to be set. In this study, at least 50% valid 2-μm DWL measurements need to be available in order to consider the averaged wind speed and wind direction for further comparison. It was verified that using a more restrictive threshold of for instance 75% or rather 90% yields comparable systematic and random errors but with a significantly reduced number of data points that can be compared. Thus, it was decided to apply a threshold of 50%.

Afterwards, all valid averaged wind speeds ($\mathrm{ws}_{2\mu m}$) and directions ($\mathrm{wd}_{2\mu m}$) are projected onto the horizontal LOS of Aeolus ($v_{2\mu\mathrm{m}_{\mathrm{HLOS}}}$) by means of the range-dependent azimuth angle $\varphi_{\mathrm{Aeolus}}$ that is provided in the Aeolus Level 2B data product according to

$$v_{2\mu\mathrm{m}_{\mathrm{HLOS}}} = \cos\left(\varphi_{\mathrm{Aeolus}} - \mathrm{wd}_{2\mu m}\right) \cdot \mathrm{ws}_{2\mu m} \tag{1}$$

In a next step, the Aeolus HLOS winds (Rayleigh-clear and Mie-cloudy) are extracted for areas of valid 2-μm DWL measurements. Beforehand, the data is filtered by means of an estimated error for the wind speeds which is also given in the Level 2B data product and which is estimated based on the measured signal levels as well as the temperature and pressure sensitivity of the Rayleigh channel response (Tan et al., 2008; Tan et al., 2017). In this study, a threshold for the estimated error of 8 m/s is applied for the Rayleigh winds and 4 m/s for the Mie winds. These thresholds are determined empirically by considering the

https://doi.org/10.5194/amt-2019-432
Preprint. Discussion started: 2 January 2020

Atmospheric Measurement Techniques Discussions

difference of Aeolus HLOS winds and 2-μm DWL winds projected onto Aeolus viewing direction (see also Eq. 2) depending on the estimated error as shown in Fig. 4. For the Rayleigh-clear winds (Fig. 4, top) it can be seen that the lowest estimated errors are calculated to be 3.7 m/s. The systematic error remains rather constant until an estimated error of about 8 m/s and then starts to increase gradually. The Mie-cloudy winds show estimated errors down to 0.7 m/s. For the Mie winds, the systematic error is rather constant up to an estimated error value of 4 m/s. For larger estimated errors, the systematic error increases remarkably. Thus, for further analysis, only Rayleigh-clear winds with estimated errors smaller than 8 m/s, and Mie-cloudy winds with estimated errors smaller than 4 m/s are considered.

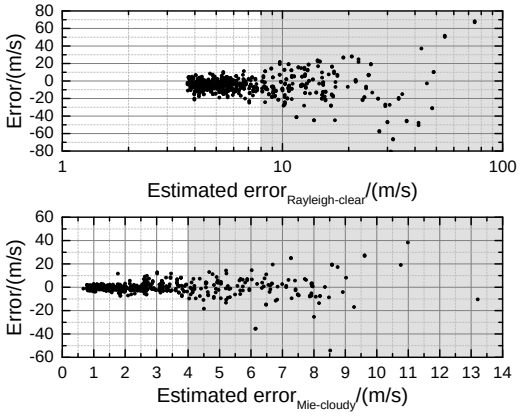

Figure 4. Difference (error) of Aeolus HLOS winds and 2-μm DWL winds projected onto Aeolus viewing direction according to Eq. (2) depending on the estimated error given in the L2B product for Rayleigh winds (top) and Mie winds (bottom). Data points with an estimated error larger than 8 m/s (Rayleigh) or rather 4 m/s (Mie) are not considered as valid observations (gray areas).

The explained averaging procedure and the resulting data sets for the 2-μm DWL and Aeolus are illustrated in Fig. 5 for the satellite underflight performed on 17 November 2018. Panel (a) indicates the wind speed retrieved from 2-μm DWL measurements, (b) shows all valid Aeolus Rayleigh-clear observations, (c) shows the 2-μm DWL data averaged to the Aeolus measurement grid and projected onto its HLOS direction, and (d) displays the corresponding Rayleigh-clear winds in regions where 2-μm DWL data is available. It can be seen that from 8719 available 2-μm DWL observations, a comparison to only 72 Rayleigh-clear observations (13 Mie-cloudy) is possible. Thus, a certain number of underflights are needed in order to get enough data points for a statistically significant comparison.

In order to validate the quality of Aeolus HLOS winds ($v_{\mathrm{Aeolus_{HLOS}}}$), the difference to the corresponding 2-μm DWL winds projected onto Aeolus viewing direction ($v_{2\mu\mathrm{m_{HLOS}}}$) is calculated according to

$$v_{\mathrm{diff_{HLOS}}} = v_{\mathrm{Aeolus_{HLOS}}} - v_{2\mu\mathrm{m_{HLOS}}} \quad (2)$$

https://doi.org/10.5194/amt-2019-432
Preprint. Discussion started: 2 January 2020

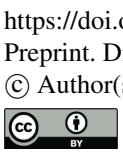

Atmospheric Measurement Techniques Discussions

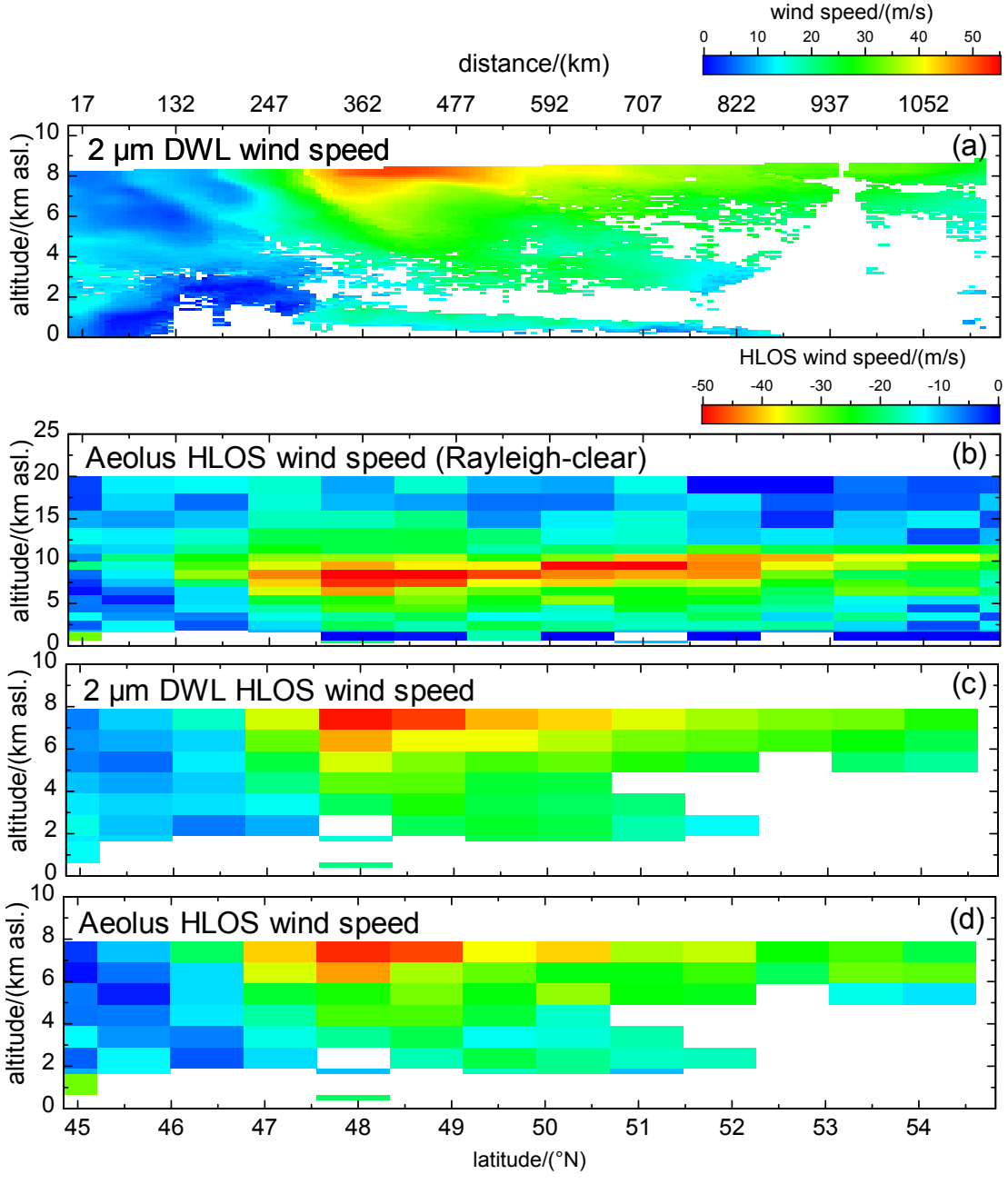

Figure 5. (a): 2-μm DWL observations obtained during the first leg of the Aeolus underflight on 17 November 2018 between 45°N and 55°N (1146 km) in the framework of the WindVal III campaign. (b): Corresponding Aeolus Rayleigh-clear winds that fulfill the quality criterion (estimated error smaller than 8 m/s). (c): 2-μm DWL observations averaged to the Aeolus grid and projected onto its viewing direction. (d): Aeolus Rayleigh-clear winds as shown in (b) in regions where 2-μm DWL data is available.

https://doi.org/10.5194/amt-2019-432
Preprint. Discussion started: 2 January 2020

Atmospheric Measurement Techniques Discussions

The bias and standard deviation (STD) of $v_{\mathrm{diff_{HLOS}}}$ are calculated by use of

$$\mathrm{bias} = \frac{1}{n}\sum_{i=1}^{n} v_{\mathrm{diff_{HLOS}}} \tag{3}$$

and

$$\mathrm{STD} = \sqrt{\frac{1}{n-1}\sum_{i=1}^{n}\left(v_{\mathrm{diff_{HLOS}}} - \mathrm{bias}\right)^2} \tag{4}$$

where n is the number of available data points. In addition to the standard deviation, the scaled median absolute deviation (scaled MAD) is calculated according to

$$\text{scaled MAD} = 1.4826 \times \mathrm{median}\left(\left|v_{\mathrm{diff_{HLOS}}} - \mathrm{median}\left(v_{\mathrm{diff_{HLOS}}}\right)\right|\right) \tag{5}$$

The scaled MAD has the advantage that it is less sensitive to single outliers which may result in larger STD values and is thus used as a measure of the random error of Aeolus HLOS winds. The scaled MAD is identical to the standard deviation (Eq. (4)) in case the analyzed data is normally distributed.

In addition to the aforementioned quantities, a least-square line-fit is performed to the respective data sets, and the retrieved slopes and intercepts are evaluated.

All Aeolus wind results in relation to the averaged 2-μm DWL wind results for both, the WindVal III and the AVATARE campaign are shown in Fig. 6, left and right, respectively and are discussed in the next section.

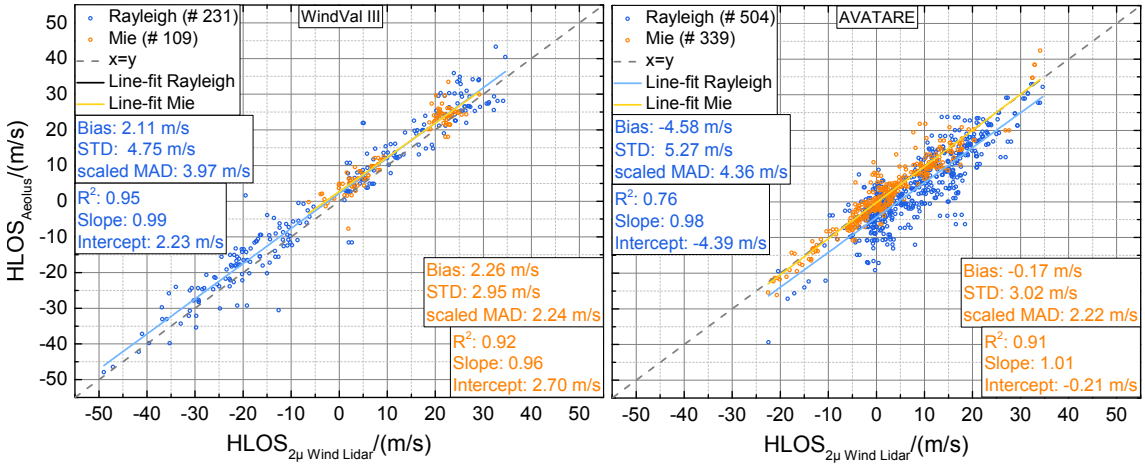

Figure 6. Aeolus HLOS wind speed plotted against the 2-μm DWL wind speed projected onto the horizontal viewing direction of Aeolus for 8 flight legs from 4 underflights performed during the WindVal III campaign 2018 (left) and for 10 flight legs from 6 underflights performed during the AVATARE campaign 2019 (right) (see also Table 1). The wind measurements are separated in Rayleigh-clear winds (blue) and Mie-cloudy winds (orange). Corresponding least-square line fits are indicated by the light blue and yellow line, respectively. The fit results are shown in the insets. The $x = y$-line is represented by the gray-dashed line.

https://doi.org/10.5194/amt-2019-432
Preprint. Discussion started: 2 January 2020


Atmospheric Measurement Techniques Discussions

6 Discussion

In Fig. 6, Rayleigh-clear winds and Mie-cloudy winds are indicated by blue dots and orange dots, respectively. Line fits to the corresponding data sets are depicted by the light blue and the yellow line. The $x = y$ - line is represented by the gray-dashed line. An summary of the statistical parameters retrieved from the scatter plot analysis is given in Table 3.

All together, the 4 satellite underflights during the WindVal III campaign resulted in 231 data points for Rayleigh-clear wind validation and 109 data points for Mie-cloudy wind validation. The 6 satellite underflights during the AVATARE campaign resulted in 504 or rather 339 data points for Rayleigh and Mie wind validation, respectively, and thus about a factor of two more than for WindVal III. The increased number of data points can be explained by two more underflights performed during the AVATARE campaign and a better 2-μm DWL performance during AVATARE due to a complete optical re-alignment of the system before the campaign leading to a remarkably better data coverage and hence to more data points being available for comparison. Additionally, since 5 March 2019 (08:44 UTC), Aeolus Mie-winds are processed with a shorter horizontal averaging length of down to 10 km also leading to more Mie winds that can be used for comparison. Furthermore, the range-gate settings of Aeolus were changed on 26 February 2019 (00:00 UTC) such that the vertical bins follow the ground elevation which also increases the number of available data points.

The slope of the least-square line fits is close to one for both campaign data sets and both wind products (Mie-cloudy and Rayleigh-clear), indicating the good correspondence of the Aeolus HLOS wind data. No significant wind speed dependent bias is obvious from the slope analysis. In particular, the slope yields 0.99 ± 0.01 (Rayleigh) and 0.96 ± 0.03 (Mie) for the WindVal III data set, and 0.98 ± 0.02 (Rayleigh) and 1.01 ± 0.02 (Mie) for the AVATARE data set. Here, the given uncertainty represents the standard error of the mean value retrieved from the least-square line-fit. In the following, the magnitude of the systematic error and the random error retrieved form both campaign data sets and potential reasons for them are discussed.

6.1 Systematic error

The intercepts of the respective line fits are determined to be (2.2 ± 0.3) m/s (Rayleigh) and (2.7 ± 0.4) m/s (Mie) for WindVal III and (-4.4 ± 0.3) m/s (Rayleigh) and (-0.21 ± 0.17) m/s (Mie) for AVATARE, where the uncertainty represents the standard error of the mean value retrieved from the least-square line-fit. Except for the Mie winds of the AVATARE data, these values are considerably larger than the specified systematic error of 0.7 m/s for Aeolus HLOS winds (ESA, 2016). A similar finding is obtained from the biases calculated according to Eq. (3) which yield 2.1 m/s (Rayleigh) and 2.3 m/s (Mie) for the WindVal III data set and -4.6 m/s (Rayleigh) and -0.17 m/s (Mie) for the AVATARE data set. Though the root-cause of the enhanced systematic error is not unequivocally verified yet, it can be explained by an inadequate calibration file that is used within the Aeolus Level 2B processor, coupled with instrumental drifts that were observed throughout the mission time (Reitebuch et al., 2019). Such kind of instrumental drifts require a regular update of the calibration file in order to avoid systematic errors in the wind retrieval which was not performed in the early-stage of the mission.

It also can be seen, that both the bias and the intercept of Rayleigh-clear winds change sign between the two campaigns, which is due to different calibration files used for the wind retrieval within the respective campaign periods. In particular,

https://doi.org/10.5194/amt-2019-432
Preprint. Discussion started: 2 January 2020


Atmospheric Measurement Techniques Discussions

since the start of the mission on 22 August 2018, the very same calibration file was used until 16 May 2019 when a different calibration file was implemented. Thus, the Aeolus data acquired in the campaigns period of WindVal III and AVATARE was processed with different calibration files, leading to the different systematic errors.

In order to further characterize and constrain the root-cause of the enhanced systematic error, its dependency on several quantities namely the time difference between 2-μm DWL and satellite observation, the actual wind speed, the scattering ratio, the altitude and the geolocation (latitude) is investigated, as shown in Fig. 7. The respective random error can be estimated by analyzing the spread of the systematic errors.

Due to the different platform speeds of the satellite (≈ 7.7 km/s) and the Falcon aircraft (≈ 200 m/s), almost all 2-μm DWL observations have a certain temporal difference with respect to the satellite observations. Depending on the variability of the atmospheric wind field, this can lead to both systematic and increased random errors for the comparison, where it is expected that both systematic and random errors increase with an increasing temporal difference between satellite and lidar observation. Thus, the obtained wind speed differences (Eq. 2) were analyzed depending on the time difference between satellite and 2-μm DWL observation as shown in Fig.7 (a). In addition to the respective observation, the mean value of 50 observations and the corresponding standard deviation (error bars) are shown for the WindVal III data set (orange) and the AVATARE data set (magenta). It can be seen that data from about 1.5 h before to 1.5 h after the satellite overflight is used for comparison. By analyzing the mean values it gets obvious that there is no significant increase of the systematic or the random error with an increasing time difference. Thus, a least-square line-fit is performed for further analysis. The determined slopes of the respective data sets are (1.1 ± 0.4) (m/s)/h for WindVal III and (0.38 ± 0.33) (m/s)/h for AVATARE. Thus, a small linear trend with respect to the time difference of the satellite overflight is obvious from the WindVal III data set, whereas no significant dependency is obvious for AVATARE. The intercept values of (2.2 ± 0.3) m/s and (-4.7 ± 0.2) m/s are comparable to the mean bias obtained for the respective data sets namely 2.1 m/s and -4.6 m/s. Hence, it is verified that the time difference between satellite and 2-μm DWL observation does not introduce a significant systematic error for the statistical analysis of the data. It also can be seen that the points scatter randomly around the mean value with a comparable spread (see also error bars of mean values), indicating that also the random error does not have a remarkable dependency on the temporal difference of Aeolus and 2-μm DWL observations.

In a next step, the dependency of the systematic error of Rayleigh-clear winds on the actual wind speed represented by the 2-μm DWL measurements is investigated as shown in Fig.7 (b). It can be seen that the acquired HLOS wind speed range was much larger for the WindVal III campaign (blue dots) ranging from -50 m/s to 35 m/s, whereas it was -20 m/s to 35 m/s for AVATARE. Least-square line-fits to the respective data sets yield a slope of -0.014 ± 0.015 and -0.022 ± 0.025 and thus would indicate a wind speed dependency of the systematic error of about 1% to 2%. However, as the uncertainty of the mean value has the same order of magnitude, this dependency is not considered significant. Additionally, the intercept of (2.2 ± 0.3) m/s and (-4.4 ± 0.3) m/s are comparable to the mean bias obtained for the respective data sets stated above.

Another interesting topic to analyze is the dependency of the systematic error of Rayleigh-clear winds on the scattering ratio given in the L2B product as shown in Fig.7 (c). It can be seen that there is a significant dependency of the systematic

https://doi.org/10.5194/amt-2019-432
Preprint. Discussion started: 2 January 2020

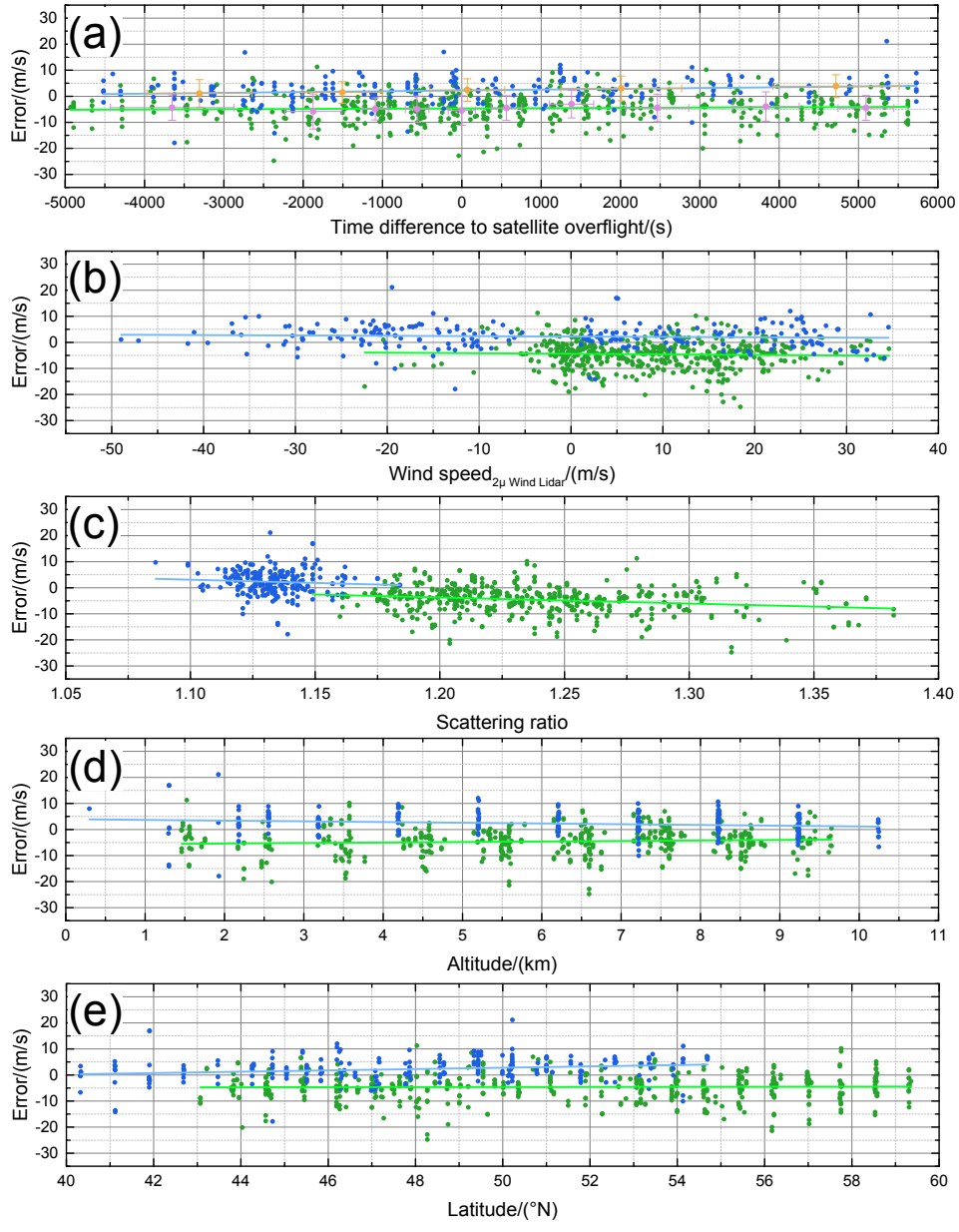

Figure 7. Systematic error of Aeolus Rayleigh-clear winds calculated according to Eq. (2) depending on time difference of 2-μm DWL observation to satellite overflight time (a), wind speed (b), scattering ratio (c) and altitude (d) and latitude (e). Data points of the WindVal III and AVATARE campaign are indicated in blue and green, respectively. Least-square line-fits to the data points are represented by the light blue and light green lines. In plot (a), the mean of 50 subsequent data points and the corresponding standard deviation (error bars) are show for WindVal III (orange) and AVATARE (magenta).

https://doi.org/10.5194/amt-2019-432
Preprint. Discussion started: 2 January 2020


Atmospheric Measurement Techniques Discussions

error on the scattering ratio for both campaign data sets. According to the least-square line-fits applied to the respective data sets, the systematic error decreases from 3.4 m/s to 1.0 m/s for WindVal III and from -2.6 m/s to -8.0 m/s for AVATARE within the available scattering ratio range. If one corrects this trend for the determined bias of 2.1 m/s (WindVal III) and -4.6 m/s (AVATARE), the systematic error is varying around zero, from -1.1 m/s to 1.3 m/s (WindVal III) or rather from -3.4 m/s to 2.0 m/s (AVATARE). Furthermore it can be seen that the scattering ratio varied between 1.08 and 1.18 for WindVal III and from 1.15 to 1.38 for AVATARE. This means that either the determination of the scattering ratio, the respective threshold for classifying Rayleigh-clear winds or rather the actual aerosol load during the flights changed between the two campaigns. The slopes of the least-square line-fits are determined to be (-24.9 ± 21.4) (m/s)/1 and (-23.2 ± 5.1) (m/s)/1 and thus even show similar magnitudes. The uncertainty of the obtained slope is smaller for the AVATARE data set as it extends over a broader scattering ratio range. A larger scattering ratio means that there is a stronger contribution of the narrow-band Mie return which also partly enters the Rayleigh spectrometer and hence results in a changed sensitivity of the Rayleigh-channel. This has to be considered for the wind retrieval in order to avoid systematic errors. Hence, it is likely that this effect is not fully corrected so far, making the scattering ratio a significant contributor of the Rayleigh-clear wind systematic error. While writing this manuscript, improvements on the scattering ratio determination and correction scheme were already ongoing in the Level 2B processor (J. de Kloe, personal communication, 7 August 2019).

The altitude dependency of the systematic error of Rayleigh-clear winds is shown in Fig.7 (d). It can be seen that the Aeolus range gate setting was kept constant during the WindVal III campaigns period (blue dots) leading to a vertical accumulation of wind observations. For the AVATARE campaign, the range gates followed the ground elevation leading to a more scattered distribution of the data points. The least-square line-fits to the respective data sets yield (-0.27 ± 0.12) (m/s)/km and (0.20 ± 0.11) (m/s)/km and thus indicate a small altitude dependency. Though it is not verified, this could be due to an imperfect temperature and pressure correction needed for the wind retrieval (Dabas et al., 2008) or an altitude dependent scattering ratio during the flights. As two different calibration files were used for the Level 2B processing of Aeolus data within the respective campaigns period, this could also explain the different slope sign for the two campaign data sets. However, more measurements would be needed in order to solidly determine if the systematic error shows a significant altitude dependency.

Lastly, the dependency of the systematic error of Rayleigh-clear winds on latitude is analyzed as indicated by Fig.7 (e). It can be seen that 2-μm DWL observations are available form 40°N to 60°N. The least-square line-fits to the respective data sets yield (0.26 ± 0.08) (m/s)/°N (WindVal III) and (0.02 ± 0.05) (m/s)/°N (AVATARE). Thus, a small latitude dependency is obvious from the WindVal III comparison, but not for AVATARE. The analysis of Aeolus ground returns, that should actually yield 0 m/s wind velocity, has shown that there is an harmonic variation of the bias along the orbital phase (latitude dependence) (Reitebuch et al., 2019). In the future, this harmonic bias will be corrected by for instance exploiting ground return signals.

In summary, besides a generally incorrect calibration file, the scattering ratio or rather the corresponding correction scheme seem to be the main contributer to the systematic error of Rayleigh-clear winds. For Mie-cloudy winds the calibration file is considered to be the main reason for the enhanced systematic error. Given the small systematic bias of Mie-cloudy winds (-0.17 m/s) for the AVATARE campaign, it can be concluded that the strict requirement of 0.7 m/s specified for Aeolus HLOS winds can principally be met.

https://doi.org/10.5194/amt-2019-432
Preprint. Discussion started: 2 January 2020

Atmospheric Measurement Techniques Discussions

6.2 Random error

The random error of Aeolus HLOS winds, represented by the scaled median absolute deviation according to Eq. (4) is determined to be 4.0 m/s (Rayleigh) and 2.2 m/s (Mie) for the WindVal III data set, and 4.4 m/s (Rayleigh) and 2.2 m/s (Mie) for the AVATARE data set. Thus, for Rayleigh-clear winds, the random error is significantly larger than the 2.5 m/s planned for Aeolus HLOS winds in altitudes between 2 km and 16 km (ESA, 2016; Kanitz et al., 2019; Reitebuch et al., 2019).

The main reason for the enhanced random error is a lower-than-expected signal level of the light backscattered from the atmosphere. On the one hand, this is caused by a lower laser pulse energy of about 53 mJ during WindVal III and 42 mJ during AVATARE instead of 80 mJ as originally planned for Aeolus (ESA, 2016; Kanitz et al., 2019; Reitebuch et al., 2019). On the other hand, slight misalignments could introduce a clipping of the laser beam within the receiver at the field stop leading to additional signal loss. Using a radiometric performance simulation tool, the detected signal levels are estimated to be a factor of 2.5 to 3 lower than expected (Reitebuch et al., 2019).

The 11 mJ decrease in laser pulse energy between the WindVal III and the AVATARE campaigns period also explains the increase in random error of the Rayleigh-clear winds from 4.0 m/s to 4.4 m/s. Considering that the random error is dominated by shot noise (Poisson noise), it is expected to scale with the square-root of the laser energy. Thus, the expected random error for AVATARE can be calculated by considering the random error determined for WindVal III (3.97 m/s) and the respective mean laser energies (53 mJ for WindVal III and 42 mJ for AVATARE) according to $4.0\,\mathrm{m/s} \cdot \sqrt{53\,\mathrm{mJ}/42\,\mathrm{mJ}} = 4.5\,\mathrm{m/s}$, which is in good accordance with the determined random error of 4.4 m/s, considering the uncertainties of the respective quantities. The Mie-cloudy wind random error does not show this trend which is due to the fact that the Mie return signal does not only depend on the laser energy but also on the presence of aerosols and clouds and their respective optical properties (backscatter and extinction coefficient) which can compensate the lower laser power.

Table 3. Comparison of Aeolus HLOS winds and 2-μm DWL winds projected onto the horizontal viewing direction of Aeolus

	Rayleigh$_{\mathrm{clear}}$					**Mie$_{\mathrm{cloudy}}$**				
	slope (m/s)/(m/s)	intercept (m/s)	Bias (m/s)	MAD (m/s)	points	Slope (m/s)/(m/s)	Intercept (m/s)	Bias (m/s)	MAD (m/s)	points
WindVal III	0.99 ± 0.01	2.2 ± 0.3	2.1	4.0	231	0.96 ± 0.03	2.7 ± 0.4	2.3	2.2	109
AVATARE	0.98 ± 0.02	-4.4 ± 0.3	-4.6	4.4	504	1.01 ± 0.02	-0.21 ± 0.17	-0.17	2.2	339

The uncertainty given for the slope and intercept values represents the standard error retrieved from the least-square line-fit.

7 Summary

DLR recently performed two airborne campaigns with two wind lidars aboard DLR's Falcon aircraft over central Europe in November/December 2018 and June/July 2019 in order to validate ESA's Aeolus mission. 10 satellite underflights with 19 flight

https://doi.org/10.5194/amt-2019-432
Preprint. Discussion started: 2 January 2020


Atmospheric Measurement Techniques Discussions

legs covering more than 7500 km of Aeolus swaths were performed and used to validate the preliminary wind data product of Aeolus by means of collocated observations for the first time.

For the WindVal III campaign, the systematic error is determined to be 2.1 m/s for Rayleigh-clear winds and 2.3 m/s for Mie-cloudy winds. For the AVATARE campaign, the systematic error is -4.6 m/s (Rayleigh-clear) and -0.2 m/s (Mie-cloudy). Except for the Mie-cloudy winds measured during the AVATARE campaign, the systematic error is remarkably larger than the 0.7 m/s planned for Aeolus. Instrumental drifts together with inadequate calibration files are presumed to be the reasons for the enhanced systematic errors, which can and will be corrected in re-processed datasets and which will be avoided for future data by improved algorithms.

Dependencies of the systematic error on observation time difference, wind speed, scattering ratio, altitude and geolocation were investigated, showing that the backscattering ratio has a remarkable influence on the systematic error. This points to an issue with the cross-talk correction within the Level 2B retrieval which is currently revised.

It is worth mentioning that the Aeolus Level 2B product used in this study is still on a early stage and will also be improved based on the results of the airborne campaigns presented in this study. A few of the mentioned and discussed issues are already solved.

The random error of Rayleigh-clear winds is determined to be 4.0 m/s (WindVal III) and 4.36 m/s (AVATARE), the one of Mie-cloudy winds to be 2.2 m/s (WindVal III) and 2.2 m/s (AVATARE). Thus, for Rayleigh-clear winds, the random error is significantly larger than the 2.5 m/s planned for Aeolus HLOS winds in altitudes between 2 km and 16 km. The enhanced random error is related to the lower laser energy together with an additional signal loss in the receiver possibly caused by clipping of the return signal on the field stop of the receiver. This also explains the even higher random error during the AVATARE campaign, where the mean laser energy was 11 mJ lower than during WindVal III.

The results elaborated in this study confirm the necessity to validate the Aeolus wind product and demonstrates that the DLR airborne wind lidar payload is well suited for this task. In September 2019, another validation campaign is planned to be flown out of Keflavik, Iceland in order to verify the performance of Aeolus in the North Atlantic region over a large wind speed range in the vicinity of the jet-stream. This is also the first opportunity to investigate the performance of the second laser of Aeolus which has been operating since July 2019 during collocated airborne wind lidar observations.

Author contributions. Benjamin Witschas prepared the main part of the manuscript and performed the statistical comparison of 2-μm DWL and Aeolus data. Christian Lemmerz was the principal investigator of both validation campaigns and supported both the analysis of lidar data and the preparation of this manuscript. Alexander Geiß supported the flight planning and performed the analysis of the meteorological conditions during the satellite underflights. Oliver Lux provided an overview of all the satellite underflights performed during both campaigns. Additionally, he helped with the statistical analysis of comparing Aeolus and 2-μm DWL data. Uwe Marksteiner provided valuable insights to the Aeolus data processor and corresponding instrument calibrations that have a tremendous impact on the retrieved wind speeds. Stephan Rahm is the principal investigator of the 2-μm DWL, processed the 2-μm DWL data and contributed to the preparation of this manuscript. Oliver Reitebuch supported the analysis of satellite data and provided valuable comments on the respective processing steps used in the Aeolus

https://doi.org/10.5194/amt-2019-432
Preprint. Discussion started: 2 January 2020

Atmospheric Measurement Techniques Discussions

processor. Additionally, he assisted in the preparation of this manuscript. Fabian Weiler provided the satellite data and did corresponding analysis and contributed to preparing this manuscript.

Competing interests. The authors declare that they have no conflict of interest.

Acknowledgements. The technical assistance by Engelbert Nagel (DLR), Sammy Henderson and Dale Bruns (Beyond Photonics) as well as the support of the DLR flight facility for the realization of the performed validation campaigns is highly acknowledged, just as the valuable comments provided by Thomas Kanitz (ESA), Michael Rennie (ECMWF), Jos de Kloe (KNMI) and Thorsten Fehr (ESA). The development of the ALADIN Airborne Demonstrator and the work carried out during the WindVal III campaign were supported by the German Aerospace Center (Deutsches Zentrum für Luft- und Raumfahrt e.V., DLR) and the European Space Agency (ESA), providing funds related to the preparation of Aeolus (WindVal III, contract no. 4000114053/15/NL/FF/gp and AVATARE, contract no. 4000128136/19/NL/ia). The authors acknowledge the provision of preliminary data (not fully calibrated/validated and not yet publicly released) of the Aeolus mission that is part of the European Space Agency (ESA) Earth Explorer Programme. Further data quality improvements, including in particular a significant product bias reduction, will be achieved before the public data release.

https://doi.org/10.5194/amt-2019-432
Preprint. Discussion started: 2 January 2020

Atmospheric Measurement Techniques Discussions

References

Ansmann, A., Wandinger, U., Le Rille, O., Lajas, D., and Straume, A.: Particle backscatter and extinction profiling with the spaceborne high-spectral-resolution Doppler lidar ALADIN: methodology and simulations, Appl. Opt., 46, 6606–6622, 2007.

Browning, K. and Wexler, R.: The determination of kinematic properties of a wind field using Doppler radar, Journal of Applied Meteorology, 7, 105–113, https://doi.org/10.1175/1520-0450(1968)007<0105:tdokpo>2.0.co;2, 1968.

Chanin, M., Garnier, A., Hauchecorne, A., and Porteneuve, J.: A Doppler lidar for measuring winds in the middle atmosphere, Geophys. Res. Lett., 16, 1273–1276, 1989.

Chouza, F., Reitebuch, O., Groß, S., Rahm, S., Freudenthaler, V., Toledano, C., and Weinzierl, B.: Retrieval of aerosol backscatter and extinction from airborne coherent Doppler wind lidar measurements, Atmospheric Measurement Techniques, 8, 2909–2926, https://doi.org/10.5194/amtd-8-1935-2015, 2015.

Chouza, F., Reitebuch, O., Jähn, M., Rahm, S., and Weinzierl, B.: Vertical wind retrieved by airborne lidar and analysis of island induced gravity waves in combination with numerical models and in situ particle measurements, Atmospheric Chemistry and Physics, 16, 4675–4692, https://doi.org/10.5194/acp-2015-1014, 2016.

Chouza, F., Witschas, B., and Reitebuch, O.: Heterodyne high-spectral-resolution lidar, Applied optics, 56, 8121–8134, 2017.

Dabas, A., Denneulin, M., Flamant, P., Loth, C., Garnier, A., and Dolfi-Bouteyre, A.: Correcting winds measured with a Rayleigh Doppler lidar from pressure and temperature effects, Tellus A, 60, 206–215, 2008.

ESA: The four candidate Earth explorer core missions: Atmospheric dynamics mission., ESA Report for Mission Selection ESA SP-, 1233, 145–pp, 1999.

ESA: ADM-Aeolus Mission Requirements Documents, AE-RP-ESA-SY-001, 2016.

Flamant, P., Cuesta, J., Denneulin, M.-L., Dabas, A., and Huber, D.: ADM-Aeolus retrieval algorithms for aerosol and cloud products, Tellus A: Dynamic Meteorology and Oceanography, 60, 273–286, 2008.

Flesia, C. and Korb, C.: Theory of the double-edge molecular technique for Doppler lidar wind measurement, Appl. Opt., 38, 432–440, 1999.

Horányi, A., Cardinali, C., Rennie, M., and Isaksen, L.: The assimilation of horizontal line-of-sight wind information into the ECMWF data assimilation and forecasting system. Part I: The assessment of wind impact, Quarterly Journal of the Royal Meteorological Society, 141, 1223–1232, 2015.

Kanitz, T., Lochard, J., Marshall, J., McGoldrick, P., Lecrenier, O., Bravetti, P., Reitebuch, O., Rennie, M., Wernham, D., and Elfving, A.: Aeolus first light: first glimpse, in: International Conference on Space Optics - ICSO 2018, vol. 11180, p. 111801R, International Society for Optics and Photonics, 2019.

Köpp, F., Rahm, S., and Smalikho, I.: Characterization of Aircraft Wake Vortices by 2-μm Pulsed Doppler Lidar, Journal of Atmospheric and Oceanic Technology, 21, 194–206, 2004.

Lux, O., Lemmerz, C., Weiler, F., Marksteiner, U., Witschas, B., Rahm, S., Schäfler, A., and Reitebuch, O.: Airborne wind lidar observations over the North Atlantic in 2016 for the pre-launch validation of the satellite mission Aeolus, Atmospheric Measurement Techniques, 11, 3297–3322, 2018.

Lux, O., Lemmerz, C., Weiler, F., Marksteiner, U., Witschas, B., Rahm, S., Geiss, A., and Reitebuch, O.: Intercomparison of tropospheric wind observations from ESA's satellite mission Aeolus and the ALADIN Airborne Demonstrator, Atmospheric Measurement Techniques Discussions, 2019, x–xx, https://doi.org/xx.xxxx/amt-2019-xxx, 2019.

https://doi.org/10.5194/amt-2019-432
Preprint. Discussion started: 2 January 2020

Atmospheric Measurement Techniques Discussions

Marksteiner, U.: Airborne wind lidar observations for the validation of the ADM-Aeolus instrument, Ph.D. thesis, Technische Universität München, 2013.

Marksteiner, U., Lemmerz, C., Lux, O., Rahm, S., Schäfler, A., Witschas, B., and Reitebuch, O.: Calibrations and Wind Observations of an Airborne Direct-Detection Wind LiDAR Supporting ESA's Aeolus Mission, Remote Sensing, 10, 2056, 2018.

Marseille, G.-J., Stoffelen, A., and Barkmeijer, J.: Impact assessment of prospective spaceborne Doppler wind lidar observation scenarios, Tellus A: Dynamic Meteorology and Oceanography, 60, 234–248, 2008.

McKay, J. A.: Assessment of a multibeam Fizeau wedge interferometer for Doppler wind lidar, Applied optics, 41, 1760–1767, 2002.

Reitebuch, O.: *Atmospheric Physics: Background - Methods - Trends*, chap. The Spaceborne Wind Lidar Mission ADM-Aeolus, pp. 487–507, Springer Berlin, Heidelberg, 2012.

Reitebuch, O., Lemmerz, C., Nagel, E., Paffrath, U., Durand, Y., Endemann, M., Fabre, F., and Chaloupy, M.: The Airborne Demonstrator for the Direct-Detection Doppler Wind Lidar ALADIN on ADM-Aeolus. Part I: Instrument Design and Comparison to Satellite Instrument, J. Atmos. Oceanic Technol., 26, 2501–2515, 2009.

Reitebuch, O., Huber, D., and Nikolaus, I.: Algorithm Theoretical Basis Document ATBD: ADM-Aeolus Level 1B Products, Tech. rep., AE-RP-DLR-L1B-001, 2014.

Reitebuch, O., Lemmerz, C., Lux, O., Marksteiner, U., Witschas, B., and Neely, R.: WindVal-Joint DLR-ESA-NASA Wind Validation for Aeolus, Final Report Contract No. 4000114053/15/NL/FF/gp, European Space Agency (ESA), Noordwijk, The Netherlands, 2017.

Reitebuch, O., Marksteiner, U., Rompel, M., Meringer, M., Schmidt, K., Huber, D., Nikolaus, I., Dabas, A., Marshall, J., de Bruin, F., et al.: Aeolus End-to-End Simulator and Wind Retrieval Algorithms up to Level 1B, in: EPJ Web of Conferences, vol. 176, p. 02010, EDP Sciences, 2018.

Reitebuch, O., Lemmerz, C., Lux, O., Marksteiner, U., Rahm, S., Weiler, F., Witschas, B., Meringer, M., Schmidt, K., Huber, D., Nikolaus, I., Geiss, A., Vaughan, M., Dabas, A., Flament, T., Stieglitz, H., Isaksen, L., Rennie, M., de Kloe, J., Marseille, G.-J., Stoffelen, A., Wernham, D., Kanitz, T., Straume, A.-G., Fehr, T., von Bismark, J., Floberghagen, R., and Parrinello, T.: Initial assessment of the performance of the first Wind Lidar in space on Aeolus, in: International Laser Radar Conference, 2019, Wuhan, China, 2019.

Rennie, M. P.: An assessment of the expected quality of Aeolus Level-2B wind products, in: EPJ Web of Conferences, vol. 176, p. 02015, EDP Sciences, 2018.

Schäfler, A., Craig, G., Wernli, H., Arbogast, P., Doyle, J. D., McTaggart-Cowan, R., Methven, J., Rivière, G., Ament, F., Boettcher, M., et al.: The North Atlantic waveguide and downstream impact experiment, Bulletin of the American Meteorological Society, 99, 1607–1637, 2018.

Smalikho, I.: Techniques of wind vector estimation from data measured with a scanning coherent Doppler lidar, Journal of Atmospheric and Oceanic Technology, 20, 276–291, 2003.

Stoffelen, A., Pailleux, J., Källén, E., Vaughan, J. M., Isaksen, L., Flamant, P., Wergen, W., Andersson, E., Schyberg, H., Culoma, A., et al.: The atmospheric dynamics mission for global wind field measurement, Bulletin of the American Meteorological Society, 86, 73–88, 2005.

Straume, A. G., Elfving, A., Wernham, D., de Bruin, F., Kanitz, T., Schuettemeyer, D., von Bismarck, J., Buscaglione, F., Lecrenier, O., and McGoldrick, P.: ESA's spaceborne lidar mission ADM-Aeolus; project status and preparations for launch, in: EPJ Web of Conferences, vol. 176, p. 04007, EDP Sciences, 2018.

Straume, A.-G., Rennie, M., Isaksen, L., de Kloe, J., Marseille, G.-J., Stoffelen, A., Flament, T., Stieglitz, H., Dabas, A., Huber, D., Reitebuch, O., Lemmerz, C., Lux, O., Marksteiner, U., Rahm, S., Weiler, F., Witschas, B., Meringer, M., Schmidt, K., Nikolaus, I., Geiss, A., Flamant, P., Kanitz, T., Wernham, D., von Bismark, J., Bley, S., Fehr, T., Floberghagen, R., and Parrinello, T.: ESA's Space-based Doppler Wind

https://doi.org/10.5194/amt-2019-432
Preprint. Discussion started: 2 January 2020

Lidar Mission Aeolus - First Wind and Aerosol Product Assessment Results, in: International Laser Radar Conference, 2019, Wuhan, China, 2019.

Tan, D., Andersson, E., Dabas, A., Poli, P., Stoffelen, A., De Kloe, J., and Huber, D.: ADM-Aeolus Level-2B/2C Processor Input/Output Data Definitions Interface Control Document, 2008.

Tan, D., Rennie, M., Andersson, E., Poli, P., Dabas, A., de Kloe, J., Marseille, G.-J., and Stoffelen, A.: Aeolus Level-2B Algorithm Theoretical Basis Document, Tech. rep., AE-TN-ECMWF-L2BP-0023, 2017.

Tan, D. G., Andersson, E., Fisher, M., and Isaksen, L.: Observing-system impact assessment using a data assimilation ensemble technique: application to the ADM–Aeolus wind profiling mission, Quarterly Journal of the Royal Meteorological Society: A journal of the atmospheric sciences, applied meteorology and physical oceanography, 133, 381–390, 2007.

Tan, D. G. H., Andersson, E., de Kloe, J., Marseille, G., Stoffelen, A., Poli, P., Denneulin, M., Dabas, A., Huber, D., Reitebuch, O., Flamant, P., Le Rille, O., and Nett, H.: The ADM-Aeolus wind retrieval algorithms, Tellus Series A, 60, 191–205, 2008.

Wagner, J., Dörnbrack, A., Rapp, M., Gisinger, S., Ehard, B., Bramberger, M., Witschas, B., Chouza, F., Rahm, S., Mallaun, C., Baumgarten, G., and Hoor, P.: Observed versus simulated mountain waves over Scandinavia – improvement of vertical winds, energy and momentum fluxes by enhanced model resolution?, Atmospheric Chemistry and Physics, 17, 4031–4052, https://doi.org/10.5194/acp-17-4031-2017, http://www.atmos-chem-phys.net/17/4031/2017/, 2017.

Weissmann, M. and Cardinali, C.: Impact of airborne Doppler lidar observations on ECMWF forecasts, Quarterly Journal of the Royal Meteorological Society: A journal of the atmospheric sciences, applied meteorology and physical oceanography, 133, 107–116, 2007.

Weissmann, M., Busen, R., Dörnbrack, A., Rahm, S., and Reitebuch, O.: Targeted observations with an airborne wind lidar, Journal of Atmospheric and Oceanic Technology, 22, 1706–1719, 2005.

Witschas, B.: Analytical model for Rayleigh–Brillouin line shapes in air: errata, Applied Optics, 50, 5758–5758, 2011a.

Witschas, B.: Experiments on spontaneous Rayleigh-Brillouin scattering in air, Ph.D. thesis, German Aerospace Center, Oberpfaffenhofen, and Friedrich-Schiller University, Jena, Germany, 2011b.

Witschas, B., Vieitez, M. O., van Duijn, E.-J., Reitebuch, O., van de Water, W., and Ubachs, W.: Spontaneous Rayleigh–Brillouin scattering of ultraviolet light in nitrogen, dry air, and moist air, Applied Optics, 49, 4217–4227, 2010.

Witschas, B., Gu, Z., and Ubachs, W.: Temperature retrieval from Rayleigh-Brillouin scattering profiles measured in air, Optics express, 22, 29 655–29 667, 2014.

Witschas, B., Rahm, S., Dörnbrack, A., Wagner, J., and Rapp, M.: Airborne wind lidar measurements of vertical and horizontal winds for the investigation of orographically induced gravity waves, Journal of Atmospheric and Oceanic Technology, 34, 1371–1386, 2017.

Zhai, X., Marksteiner, U., Weiler, F., Lemmerz, C., Lux, O., Witschas, B., and Reitebuch, O.: Rayleigh wind retrieval for the ALADIN airborne demonstrator of the Aeolus mission using simulated response calibration, Atmospheric Measurement Techniques Discussions, 2019, 1–33, https://doi.org/10.5194/amt-2019-274, https://www.atmos-meas-tech-discuss.net/amt-2019-274/, 2019.